Received: 9 October 2019 | Revised: 26 November 2019 | Accepted: 2 December 2019

DOI: 10.1111/jace.16949

Journal of the American Ceramic Society

RAPID COMMUNICATION

Field-assisted heating of Gd-doped ceria thin film

Xin Li Phuah[1] | **Han Wang**[1] | **Zhimin Qi**[1] | **Shikhar Misra**[1] | **Matias Kalaswad**[2] | **Haiyan Wang**[1,2]

[1]School of Materials Engineering, Purdue University, West Lafayette, IN, USA

[2]School of Electrical and Computer Engineering, Purdue University, West Lafayette, IN, USA

Correspondence
Haiyan Wang, School of Materials Engineering, Purdue University, West Lafayette, IN 47907, USA.
Email: hwang00@purdue.edu

Funding information
Office of Naval Research, Grant/Award Number: N00014-16-1-2778 and N00014-17-1-2087; US National Science Foundation, Grant/Award Number: DMR-1809520, DMR and -1565822; Purdue Doctoral Fellowship

Abstract

Flash sintering has recently been used to sinter various bulk ceramics under reduced sintering temperatures and sintering time by applying an electric field across the sample. In this work, we have demonstrated field-assisted heating of 10 mol% Gd-doped CeO_2 thin films deposited by pulsed laser deposition. Microstructure analysis revealed the elongated grains aligned in the out-of-plane direction which is perpendicular to the direction of electric field. The overall microstructure of the flash-heated thin film also contained a matrix of porous and clustered regions, which are distributed throughout the thin film from the anode to cathode electrode regions. The flash-heated thin film showed significantly different conductivity and optical permittivity compared to the as-grown thin films. This demonstration suggests a feasible approach for post-deposition synthesis of thin films using field-assisted heating toward novel morphologies and properties.

KEYWORDS

conductivity, flash sintering, microstructure, permittivity, thin films

1 | INTRODUCTION

Flash sintering of bulk ceramics has gained significant attention since the first demonstration in 2010,[1] as bulk ceramics can be effectively densified within seconds at lower furnace temperatures than that of conventional sintering. This sintering technique uses a strong applied field across the sample during heating. Since ceramics have a negative temperature coefficient of resistivity, increasing the furnace temperature leads to an increase in the conductivity of the sample. At the onset temperature,[2] there will be sufficient conductivity to allow current flow through the green body and abrupt densification of the green body follows.[3] At this point, the mechanism is still unclear and several hypotheses have been proposed, including Joule heating,[4,5] Frenkel pair formation,[1] electrochemical reactions,[6] and grain boundary overheating or melting.[7,8]

The extreme densification rate and the presence of an electric field during flash sintering have led to nonequilibrium characteristics in various flash-sintered bulk ceramics. For example, in situ synchrotron studies[9] have observed metastable phase transformations[10,11] and abnormal lattice expansions across the sample[12,13] during flash sintering. Microstructure characterization after flash sintering revealed asymmetric grain growth,[14–16] texturing,[3,17] and high density of defects,[3,17,18] as a result of the generation and mobility of the charged species caused by the applied DC field. In conventional sintering, bulk ceramics typically do not have any these unique characteristics.

One of the main challenges yet is the implementation of flash sintering for new applications and technological advances beyond the bulk ceramic sintering. A recent study has demonstrated the flash sintering of ceramic films with varying thicknesses in the range of sub-millimeters.[19] Other efforts include reactive flash sintering for rapid chemical synthesis of complex single phase oxides.[20,21] However, flash sintering performed on thin films has yet to be demonstrated and could open new opportunities in various solid-state device applications, such as fuel cells and batteries. Hence, the present work is to demonstrate the feasibility of performing a

modified version of flash sintering on thin films and explore the potential of flash sintering in altering the film morphology and physical properties.

2 | EXPERIMENTAL PROCEDURE

For the thin film deposition, the target of 10 mol% Gd-doped CeO_2 (GDC) was prepared by a solid-state sintering method. The thin films were deposited on single-crystal (001)-oriented $SrTiO_3$ (STO) substrates by pulsed laser deposition (PLD) using a KrF excimer laser ($\lambda = 248$ nm). All depositions were performed under 200 mTorr oxygen and at a deposition temperature of 300°C. After the deposition, the thin films were annealed under 500 Torr oxygen for 30 minutes and then cooled down to room temperature.

The thin film specimens were analyzed by X-ray diffraction (XRD, PANalytical Empyrean). Transmission electron microscope (TEM, FEI TALOS F200X) operated at 200 kV was used for microstructure characterization. For TEM observation, the thin film specimens were sectioned, mechanically ground and dimpled, followed by ion polishing in a precision ion milling system (PIPS II, Gatan). For the flash-heated thin film, the TEM sample was prepared near the anode electrode. The surface morphology of the thin film from the anode to cathode end was imaged by scanning electron microscope (SEM, FEI Quanta 650). The electrical conductivity of the thin films was measured by impedance analyzer (Gamry series G300 Potentiostat) in the frequency range of 100 mHz to 30 kHz with the temperature ranging from 300°C to 1000°C. The dielectric permittivity of the thin films was measured using a spectroscopic ellipsometer (JA Woollam RC2). The ellipsometer parameters ψ and Δ were fitted using a mix of Lorentz and Tauc-Lorentz oscillators to enforce the Kramers-Kronig consistency.

Figure 1A shows the experimental setup used to perform field-assisted heating of thin films. Similar to bulk flash sintering, the two ends of the thin film were connected to a power supply to apply an electrical field. Platinum contacts were deposited at the ends of a rectangular alumina substrate to create an electrode holder. Platinum wires were inserted in a small slit of the electrode holder and connected to a power supply. Platinum paste was used on the thin film in contact with the electrode holder to ensure good electrical contacts. The furnace was heated to 900°C at a heating rate of 10°C/min while a voltage of 150 V (electric field is ~150 V/cm for a 1 cm substrate) was applied. As the specimen became conductive, the current increased rapidly up to a steady state and was held for 90 seconds before turning the power supply off.

Figure 1B shows the electrical voltage and current data collected during the field-assisted heating process. Around 79 minutes, where the furnace temperature reached 875°C, the current abruptly increased to a maximum of 36 mA and stayed constant at 32 mA. The power supply did not require switching to a current control as the current stayed constant and did not increase indefinitely, unlike typical flash sintering of bulk samples. During the flash sintering of bulk ceramics, the current increase is typically correlated with the densification of the sample.[3] Figure 1C shows a snapshot of the sample glowing when the current began to flow through the thin film. In previous flash sintering studies, this event has been commonly observed and the photoemission has been explained as a result of thermal radiation[22] and/or electroluminescent phenomena.[23] The video of the sample right before and during field-assisted heating event is available in the supplementary material.

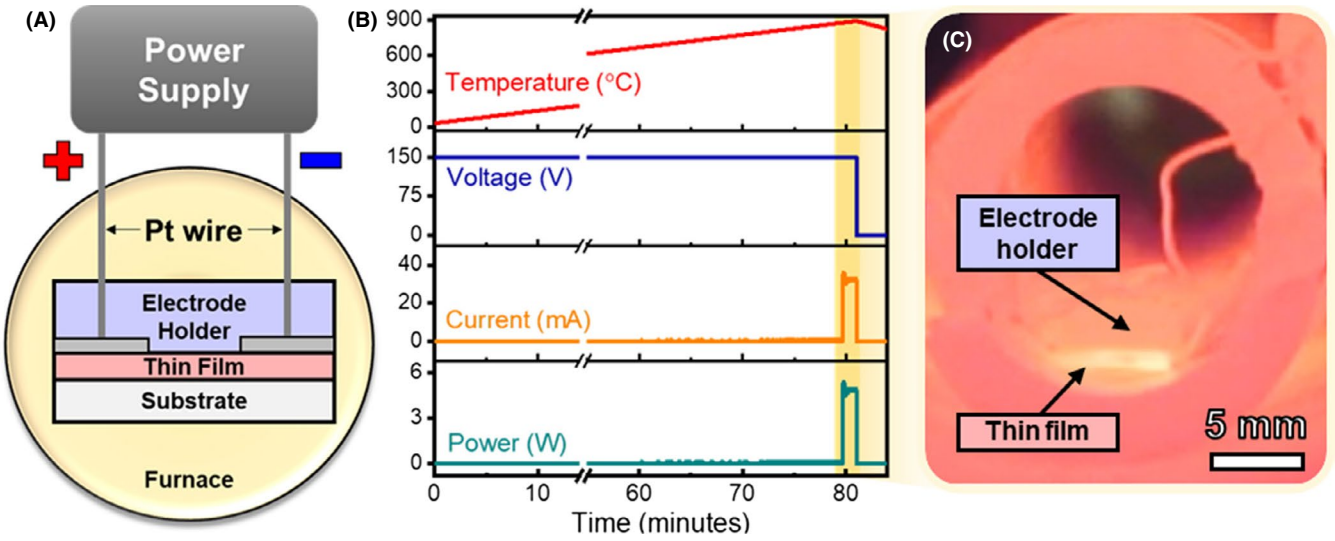

FIGURE 1 A, Schematic of the experimental setup for thin film flash sintering. B, Electrical data collected from the power supply during the flash sintering of GDC thin film. C, Photograph of the thin film sample glowing during flash sintering when the current began to flow around 79 min ($T_{furnace}$ ~ 875°C) [Color figure can be viewed at wileyonlinelibrary.com]

3 | RESULTS AND DISCUSSION

Figure 2A-C shows the XRD θ-2θ of the as-grown, no-field, and flash-heated GDC thin films, respectively. The "no-field" sample was heated in the furnace with the same conditions as the flash-sintered thin film, but without any field applied. This enables the separation of the heating effect and any additional effect(s) introduced by field-assisted heating. Comparing the GDC (111) peak, the width of the peak starts to diminish for the no-field thin film and even more for the flash-sintered thin film. Since the full width half maximum (FWHM) is inversely proportional to the crystallite size,[24] the grain size for the no-field sample is larger than the as-grown GDC, and the grain size of the flash-sintered is even larger than that of the no-field.

Figure 2D-F shows the TEM cross-sectional images and the corresponding selected area diffraction (SAD) pattern of the as-grown, no-field, and flash-heated GDC thin films, respectively. Since the as-grown GDC was deposited at low temperatures, the film thickness is approximately 185 nm and the overall structure is porous with average grain size of ~2 nm. The no-field GDC had significant coarsening and the grain size grew to about ~25 nm without any change to the film thickness. The flash-heated GDC demonstrated the largest average grain size up to ~35 nm and a slight decrease in film thickness. The change in film thickness could be a result of additional Joule heating which increased the sample temperature and led to some densification of particles. The SAD patterns correspond well with the difference in grain size, where the larger grain size has less distinguished diffraction dots. The structure is rather unique as it has a single layer of well-connected grains right at the surface of the substrate while the grains above the layer are in columnar grain fashion and elongated in the out-of-plane direction, which is perpendicular to the direction of the applied field. Such a unique vertically aligned porous structure presents potential to be used as a porous cathode in solid oxide fuel cells (SOFC), as it could improve the rates of gas transport through the cathodes.[25]

Figure 3A shows the scanning transmission electron microscopy (STEM) images of the overall cross-sectional morphology for the flash-heated GDC. Two distinct characteristics were identified; the majority of the thin film contained (a1) porous regions and (a2) cluster regions appearing every few microns. The porous regions have very limited connectivity in-plane with other grains while these cluster regions are very dense but still elongated in the same direction. The formation of these clusters has not been reported in flash-sintered bulk ceramics.

To analyze the distribution of clusters within the flash-heated GDC thin film, the surface morphology was also investigated by scanning electron microscopy (SEM) imaging. Figure 3B shows measured cluster size and cluster density captured from surface images of the thin film from the anode to the cathode end. The largest cluster size was found in the middle of the sample but the highest cluster density was observed near the anode end. It is likely that the middle section had larger cluster size since that section experienced less heat loss to the surroundings compared to the electrode ends, resulting in increased coarsening. On the contrary, the asymmetric distribution is likely related to the electric field, as it has shown to affect the grain growth behavior between the anode and cathode electrodes.[6,12,14–16,26]

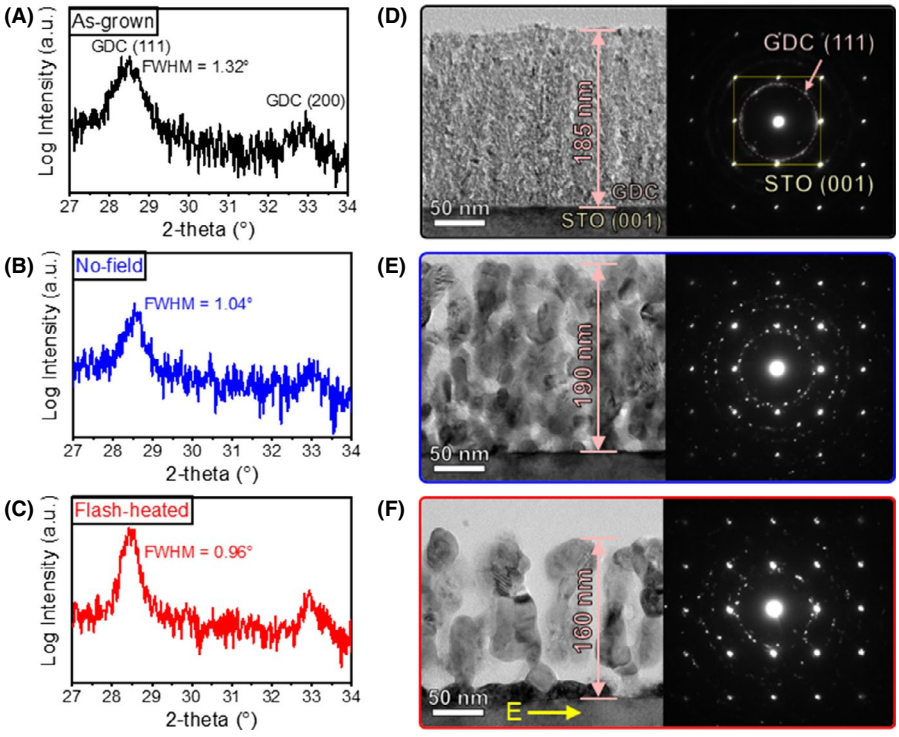

FIGURE 2 XRD θ-2θ of the thin film samples (A) as-grown, (B) no-field applied (only heating), and (C) flash-heated. TEM of the cross-sectional area is shown for the GDC thin film (D) as-grown, (E) no-field applied, and (F) flash-heated on STO substrate. The corresponding SAD is shown on the right. The direction of the electric field is labeled with "E." [Color figure can be viewed at wileyonlinelibrary.com]

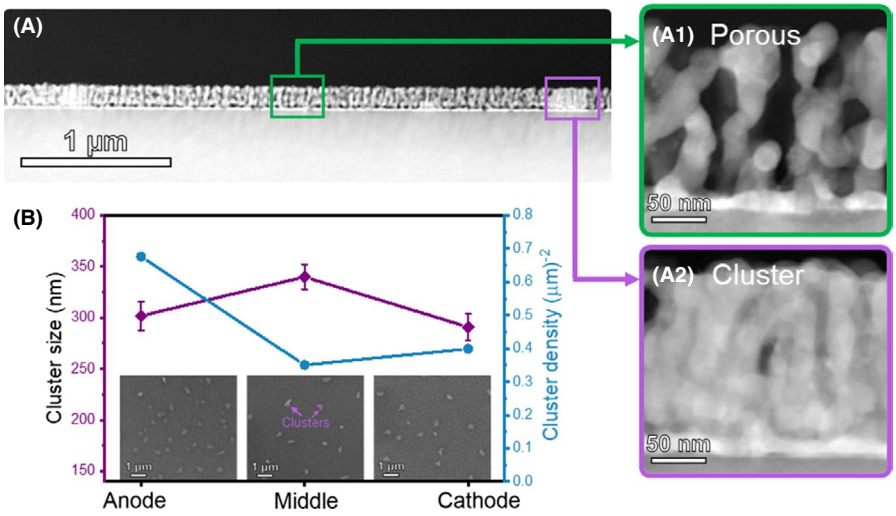

FIGURE 3 A, STEM images from the anode side showing the (A1) porous and (A2) cluster regions of the flash-heated thin film. B, Plot showing the measured cluster size and cluster density from anode to cathode ends based on secondary electron micrographs [Color figure can be viewed at wileyonlinelibrary.com]

Figure 4A shows the temperature dependence of the conductivity of the three thin film specimens based on in-plane measurements. The activation energies were estimated based on the linear fitting of the Arrhenius plots. Between 500°C and 600°C, there is a sudden change in the slope in all the fitted lines where the activation energy becomes higher and less temperature-dependent. This may suggest a change in conductivity behavior, where the conducting species are likely electrons or holes[27,28] rather than O^{2-}/Gd^{3+} ions.[29] In the lower temperature regime (300°C to 500°C), there is an obvious difference in the conductivities of the thin films. The activation energy of the as-grown GDC in the low-temperature regime matches with the bulk migration energy of $V_O^{\cdot\cdot}$ (~0.6 eV),[28] revealing the grain-to-grain conduction pathways. This can help explain the differences in the low-temperature regime conductivity, which is related to the grain morphology, as large porosities and minimal grain connectivity in the in-plane direction caused the conductivity for the flash-heated GDC to decrease at lower temperatures. However, in the high-temperature regime (600°C to 1000°C), the conductivity characteristics are quite similar for all three samples, which suggests that high-temperature conductivity is primarily attributed to bulk ionic conductivity of GDC. Overall, the flash heating process significantly impacts the low-temperature regime, that is, the electronic conductivity regime, but not the bulk ionic conductivity.

Figure 4B shows the dielectric permittivity for as-grown, no-field, and flash-heated GDC thin films obtained by fitting the angular-dependent ellipsometer data. All samples exhibited dispersion characteristic of a dielectric. The no-field GDC demonstrated a very similar permittivity to the as-grown GDC, while the flash-heated GDC showed a much lower permittivity compared to both of the as-grown and no-field GDC thin films. This implies that by utilizing field-assisted heating, the dielectric permittivity of the GDC

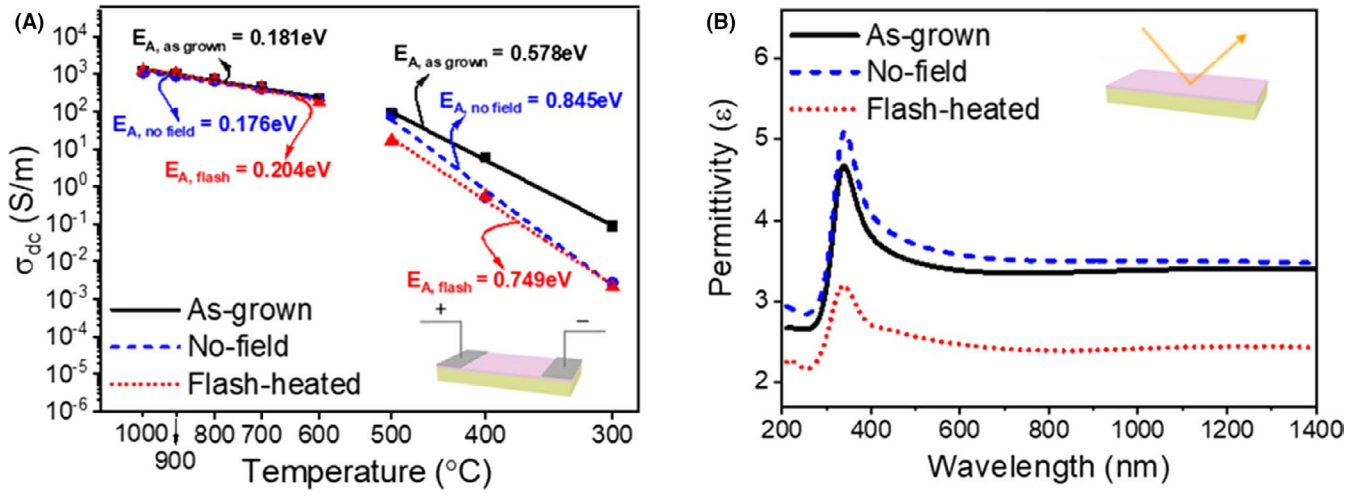

FIGURE 4 A, Arrhenius plot of conductivity and temperature of the thin film specimens. The activation energy is calculated based on the linear fitting of the points. B, Dielectric permittivity of the thin film specimens by angular-dependent ellipsometry [Color figure can be viewed at wileyonlinelibrary.com]

thin film can be effectively tuned. The decrease in dielectric permittivity for the flash-heated GDC could be attributed to the improved conductivity of the thin film after flash heating.

Another important discussion to include in this study is on the current pathway. In this experimental setup, the electrical contacts are placed on top of the thin film. The current will flow through the most conductive pathway. The STO substrate has a much lower conductivity compared to the Gd-doped CeO_2 thin film, which suggests that the current prefers to flow through the thin film. This is evident by the major microstructural changes in the thin film which are not observed in the no-field sample. It is also possible and likely for the current to preferentially flow through the film-substrate interface region in the thin film. As evident in the cross-sectional TEM images, there is a single layer of well-connected grains right above the substrate. Additionally, the elongated grains in the out-of-plane direction have poor connectivity and would also suggest the current pathway to be in the interface region.

This preliminary study introduces a new application of flash sintering and will bring many exciting opportunities for morphology tuning in thin films. There are still several challenges remaining and questions to be addressed. With the current experimental setup, achieving high reproducibility is challenging since the current increases to a certain maximum value in the milliamp range. Any slight deviation in experimental conditions could easily impact the resulting flash behavior, such as minor changes in electrical contacts and homogeneity of the as-grown thin film. Additionally, the maximum current value reached by the thin film during the flash onset is much smaller than that of typical bulk samples and this may require a feedback loop with much smaller step size and a much lower current limit for proper control.

4 | CONCLUSIONS

This work demonstrates the feasibility of post-deposition film morphology and property tuning via the field-assisted heating approach. Field-assisted heating present a very unique way to change the morphology of thin films which could not be achieved by typical thermal treatments or deposition conditions. The nanocrystalline grains in the as-grown thin film were transformed into elongated grains perpendicular to the direction of the electric field, and formed a matrix of porous and clustering structures. Similar to flash sintering of bulk ceramics, there is an asymmetric microstructure characteristic across the thin film, where the cluster size and area density varied from the anode to cathode electrode. There could be even more potential to tune the morphology if the flash-sintering parameters varied. Furthermore, there are many different material systems to explore, including various unique multilayer structures and nanocomposites. Implementing field-assisted heating could be a simple and useful technique to transform thin films after deposition.

ACKNOWLEDGMENTS

X. P., Han W., Z. Q., and H. W. acknowledge the support from the US Office of Naval Research (Contract number: N00014-17-1-2087 for flash sintering effort, N00014-16-1-2778 for TEM and N00014-16-1-2465 for the EIS work). SM acknowledges the support from the US National Science Foundation (DMR-1809520). MK acknowledges the Purdue Doctoral Fellowship and the US National Science Foundation (AGEP-GRS support under Ceramic Program, DMR-1565822).

ORCID

Xin Li Phuah https://orcid.org/0000-0001-9950-9445
Han Wang https://orcid.org/0000-0002-6137-4802
Zhimin Qi https://orcid.org/0000-0002-8154-2850
Shikhar Misra https://orcid.org/0000-0001-8257-2878
Haiyan Wang https://orcid.org/0000-0002-7397-1209

REFERENCES

1. Cologna M, Rashkova B, Raj R. Flash sintering of nanograin zirconia in <5 s at 850°C. J Am Ceram Soc. 2010;93(11):3556–9.
2. Dong Y, Chen IW. Predicting the onset of flash sintering. J Am Ceram Soc. 2015;98(8):2333–5.
3. Phuah XL, Wang H, Charalambous H, Jha SK, Tsakalakos T, Zhang X, et al. Comparison of the grain growth behavior and defect structures of flash sintered ZnO with and without controlled current ramp. Scr Mater. 2019;162:251–5.
4. Raj R. Joule heating during flash-sintering. J Eur Ceram Soc. 2012;32(10):2293–301.
5. Todd RI, Zapata-Solvas E, Bonilla RS, Sneddon T, Wilshaw PR. Electrical characteristics of flash sintering: thermal runaway of Joule heating. J Eur Ceram Soc. 2015;35(6):1865–77.
6. Biesuz M, Pinter L, Saunders T, Reece M, Binner J, Sglavo V, et al. Investigation of electrochemical, optical and thermal effects during flash sintering of 8YSZ. Materials (Basel). 2018;11(7):1214.
7. Narayan J. A new mechanism for field-assisted processing and flash sintering of materials. Scr Mater. 2013;69(2):107–11.
8. Chaim R. Liquid film capillary mechanism for densification of ceramic powders during flash sintering. Materials (Basel). 2016;9(4):19–21.
9. Jha SK, Phuah XL, Luo J, Grigoropoulos CP, Wang H, García E, et al. The effects of external fields in ceramic sintering. J Am Ceram Soc. 2018;102(1):5–31.
10. Charalambous H, Jha SK, Vikrant KSN, Garcia RE, Phuah XL, Wang H, et al.Grain boundary stabilized zirconium monoxide under DC electric-field. Under review.
11. Jha SK, Lebrun JM, Raj R. Phase transformation in the alumina-titania system during flash sintering experiments. J Eur Ceram Soc. 2016;36(3):733–9.
12. Jha SK, Charalambous H, Wang H, Phuah XL, Mead C, Okasinski J, et al. In-situ observation of oxygen mobility and abnormal lattice expansion in ceria during flash sintering. Ceram Int. 2018;44(13):15362–9.
13. Charalambous H, Jha SK, Phuah XL, Wang H, Wang H, Okasinski JS, et al. In situ measurement of temperature and reduction of rutile

titania using energy dispersive x-ray diffraction. J Eur Ceram Soc. 2018;38(16):5503–11.
14. Rheinheimer W, Phuah XL, Wang H, Lemke F, Hoffmann MJ, Wang H. The role of point defects and defect gradients in flash sintering of perovskite oxides. Acta Mater. 2019;165:398–408.
15. Zhang Y, Jung J-I, Luo J. Thermal runaway, flash sintering and asymmetrical microstructural development of ZnO and ZnO–Bi_2O_3 under direct currents. Acta Mater. 2015;94:87–100.
16. Charalambous H, Jha SK, Wang H, Phuah XL, Wang H, Tsakalakos T. Inhomogeneous reduction and its relation to grain growth of titania during flash sintering. Scr Mater. 2018;155:37–40.
17. Wang H, Phuah XL, Li J, Holland TB, Vikrant K, Li Q, et al. Key microstructural characteristics in flash sintered 3YSZ critical for enhanced sintering process. Ceram Int. 2018;45(1):1251–7.
18. Wang H, Phuah XL, Charalambous H, Jha SK, Li J, Tsakalakos T, et al. Staged microstructural study of flash sintered titania. Materialia. 2019;8:100451.
19. Avila V, Raj R. Flash sintering of ceramic films: The influence of surface to volume ratio. J Am Ceram Soc. 2019;102(6):3063–9.
20. Kok D, Yadav D, Sortino E, McCormack SJ, Tseng K-P, Kriven WM, et al. α-alumina and spinel react into single phase high-alumina spinel in < 3 seconds during flash sintering. J Am Ceram Soc. 2017;100(7):3262–8.
21. Avila V, Raj R. Reactive flash sintering of powders of four constituents into a single phase of a complex oxide in a few seconds below 700°C. J Am Ceram Soc. 2019;102(11):6443–8. https://doi.org/10.1111/jace.16625.
22. Sglavo VM, Quaranta A, Biesuz M, Luchi P, Martucci A. Photoemission during flash sintering: an interpretation based on thermal radiation. J Eur Ceram Soc. 2017;37(9):3125–30.
23. Lebrun JM, Raj R. A first report of photoemission in experiments related to flash sintering. J Am Ceram Soc. 2014;97(8):2427–30.
24. Patterson AL. The scherrer formula for X-ray particle size determination. Phys Rev. 1939;56(10):978–82.
25. Tanner CW. The effect of porous composite electrode structure on solid oxide fuel cell performance. J Electrochem Soc. 1997;144(1):21.
26. Pinter L, Biesuz M, Sglavo VM, Saunders T, Binner J, Reece M, et al. DC-electro softening in soda lime silicate glass: an electro-thermal analysis. Scr Mater. 2018;151:14–8.
27. Jiang T, Wang Z, Zhang J, Hao X, Rooney D, Liu Y, et al. Understanding the flash sintering of rare-earth-doped ceria for solid oxide fuel cell. J Am Ceram Soc. 2015;98(6):1717–23.
28. Kim S, Maier J. On the conductivity mechanism of nanocrystalline ceria. J Electrochem Soc. 2002;149(10):J73.
29. Biesuz M, Dell'Agli G, Spiridigliozzi L, Ferone C, Sglavo VM. Conventional and field-assisted sintering of nanosized Gd-doped ceria synthesized by co-precipitation. Ceram Int. 2016;42(10):11766–71.

SUPPORTING INFORMATION

Additional supporting information may be found online in the Supporting Information section.

How to cite this article: Phuah XL, Wang H, Qi Z, Misra S, Kalaswad M, Wang H. Field-assisted heating of Gd-doped ceria thin film. *J Am Ceram Soc.* 2020;103:2309–2314. https://doi.org/10.1111/jace.16949